Available online at www.sciencedirect.com
ScienceDirect
Cement and Concrete Research 36 (2006) 1483 – 1489
Cement and Concrete Research

Characterisation of 'Hadley' grains by confocal microscopy

M.K. Head *, H.S. Wong, N.R. Buenfeld

Concrete Durability Group, Department of Civil and Environmental Engineering, Imperial College London, SW7 2BU, UK

Received 31 August 2005; accepted 15 December 2005

Abstract

This work forms part of an exploratory study to investigate the use of fluorescent laser scanning confocal microscopy (LSCM) for imaging pores and voids in hardened mortar and concrete. The study has revealed the suitability of the technique for the characterisation of hollow shell (Hadley) hydration grains (these are grains that contain a void within the original boundary of the cement grain). It was found that Hadley grains could be imaged using fluorescent light techniques, subsequent to their impregnation by epoxy resin doped with a fluorescent dye. Prior to this work, it was not clear whether hollow grains were impregnated due to connections with capillary pores, or if they had been impregnated due to connections with damage caused during surface preparation (i.e. micro-cracks or deep surface scratches). However using the 3D LSCM imaging technique it was observed that connections between Hadley grains and hardened cement paste (HCP) capillary pores did exist, in different forms, at depths well below the surface providing 'conduits' along which resin was able to flow and impregnate the hollow grains. Other aspects of imaging Hadley grains are also described, such as the sectioning of 'tips' of larger grains often taken as separate smaller pores or grains in 2D images.

Keywords: 3D laser scanning confocal microscopy; Characterisation; Backscattered electron imaging

1. Introduction

The hardened cement paste in concrete contains different types of pore, with sizes that cover several orders of magnitude from the nanometre to the millimetre scale. Porosity is an important phase as it influences not only mechanical strength, but also shrinkage, creep and molecular transport. Pores are conventionally classified as, in the order of decreasing size: entrapped air, entrained air, capillary pores and gel pores. Cracks may also exist, and these are differentiated according to their size and origin. Another distinct type of pore is the hollow-shell hydration grain, also known as Hadley grain, after the discoverer [1].

Hollow-shells are hydrated cement grains that contain a void within the original boundary of the cement grain. In his Ph.D. thesis, Hadley [1] observed that a shell of hydration product forms on hydrating cement grains at early ages. As hydration continues, a progressively larger void space develops within the shell. Most of the hydration shells eventually become completely hollow, while some contain remnants of anhydrous particles. This observation is not consistent with early hydration models [2] that predicted the deposition of hydration products both inside the original cement grain boundary (inner product) and outside in the original water-filled spaces between cement grains (outer-product). Later studies using backscattered electron imaging (BEI) confirmed that hollow-shells are indeed a characteristic feature of cement hydration, and that inner product progressively replaces the space left by the hydrating anhydrous cement grain as seen in some older concretes, although the type of inner product and quantity may vary depending on whether mineral admixtures have been used during the manufacture of the concrete [3–7].

According to Diamond [8], cement grains form a shell of hydration products around themselves during the first few hours of hydration. The shell is approximately 1 μm thick, and is composed of calcium silicate hydrate (C–S–H) gel, with some calcium hydroxide (CH) and occasionally extensions of ettringite needles of thin monosulphate (or monosulphoaluminate) plates [8]. During subsequent hydration, the shell may

* Corresponding author. Tel.: +44 207 594 5956; fax: +44 207 225 2716.
E-mail address: m.head@imperial.ac.uk (M.K. Head).

0008-8846/$ - see front matter © 2006 Elsevier Ltd. All rights reserved.
doi:10.1016/j.cemconres.2005.12.020

either deposit inner hydration products, forming what is known as a 'Williamson grain' [9], or, empty-out in a hollow-shell mode and precipitate hydration products in the capillary pores between adjacent shells. Diamond [8] suggested that whether a cement grain develops into a Williamson or a Hadley grain depends on the amount of pore-solution filled space in the vicinity. The hollow-shell mode appears to be favoured where pore-solution filled spaces are available, for example near the interfacial transition zone (ITZ), while the Williamson grain development appears to predominate in dense areas, for example in closely packed cement grains. It should be noted that the interfacial zone also contains a significant number of smaller sized anhydrous grains [10,11], and thus not surprisingly that Hadley observed many hollow shells completely empty in the interfacial zone due to probably both a higher porosity and smaller sized anhydrous grains. This is supported by the findings of Kjellsen et al. [5], who observed that smaller cement grains will hydrate completely by 1 day, leaving complete hollow-shells. Larger cement grains may leave hollow-shells with a remnant anhydrous core. However, it is possible that some of the apparently completely hollow shells are, in fact, corners of larger hollow-shells containing anhydrous cores.

Hadley grains are ubiquitous in hydrated cement paste, but their nature, process of formation and influence on bulk properties of cement-based materials is imperfectly understood. Part of the reason for this is that previous microscopical studies on Hadley grains have always been limited by the two-dimensional characteristic of electron microscopy. Therefore, this paper presents an attempt to explore the nature of Hadley grains, in three-dimensions, via fluorescent laser scanning confocal microscopy (LSCM). A particular focus of this study is the interconnection between hollow-shell voids and the surrounding capillary pores, which was first reported in a paper on the feasibility of using LSCM for imaging the pore structure of cement-based materials [12]. This work described some of the technical aspects of imaging with LSCM, and reported that limited imaging of porous features in the immediate sub-surface of hardened cement pastes (HCP) was possible, but that probe signal and image resolution/clarity was lost with depth (after about 12 μm or so). Lateral resolution of the system was about 0.15 to 0.2 μm, and lateral resolution was about 0.3 μm. However, the technique is far from being fully developed for the examination of cementitious materials, and work is on-going in this respect. Previous applications of LSCM to the study of cementitious materials have been reported in the literature but none have concentrated on the pores cracks and voids of HCP, instead, employing reflected light techniques to examine surface roughness [13], and hydration products and glass bead interfaces [14–16]. Other materials applications have included the study of pores in rocks, by geologists wishing to characterise potential hydro-carbon reservoir rocks [17–20]. LSCM was mainly developed for the imaging of biological tissues, and is well-established in the bio-sciences where a large range of confocal fluorescent techniques are available. We have described some of these applications previously [12]. This however falls outside the scope of this paper and the reader is directed towards the many texts available on the subject.

2. Experimental: technique

Two concrete mixtures were studied. Specimens were manufactured with water/cement ratios (w/c) of 0.4 and 0.6, comprising of ordinary Portland cement (OPC), medium graded siliceous sand and Thames Valley gravel. Mixture proportions were 1 : 2 : 3.14 (cement : sand : gravel) for the 0.4 w/c concrete, and 1 : 2.7 : 4 for the 0.6 w/c concrete. Cylindrical specimens (100 ∅ × 250 mm) were cast and demoulded after 24 h, sealed in cling film and cured at 20 °C for 3 or 28 days. After each curing age, a 10 mm thick disc was cut from each cylinder at approximately 100 mm from the bottom cast face, from which a block specimen (40 × 20 × 10 mm) was prepared for microscopy. The blocks were freeze-dried and vacuum-impregnated with a low viscosity epoxy resin doped with fluorescent dye. They were then ground using silicon carbide papers of successively finer grit size and finally polished with cloths embedded with successively finer diamond abrasives down to 1/4 μm. Each grinding and polishing step was done at 70 rpm and a 7 N force was applied to the specimens. Polishing time was kept short (~5 min) to minimise relief. A non-aqueous solution was used as lubricant for cutting and polishing. Acetone was used as cleaning fluid.

Prior to confocal imaging, the specimens were mounted uncoated in a low vacuum SEM, and imaged in backscattered electron mode. Images were captured at various magnifications ranging from ×100 to ×1000. The images were printed and used as an aid in relocating the same areas with the confocal microscope. Confocal data capture involves sequential imaging through the Z-axis by incrementally stepping the specimen through the focal plane of the objective lens (moving the specimen towards the lens has the effect of shifting the focal plane deeper into the specimen). The resulting image stack can be loaded into computer memory and manipulated to produce 3D projections and models. Unlike backscattered electron images however, confocal epi-fluorescent images contrast only resin-filled voids against solid non-impregnated fractions of the material. Therefore the BEI image shown in Fig. 1a was captured to help explain and correctly identify dark regions of a corresponding confocal image (Fig. 1b). Also indicated in Fig. 1a and b are some of the many hollow shell grains present in the images (marked 1–6). These are some of the larger grains. Smaller apparently fully hydrated grains can be observed in all parts of the images, most noticeably in the top half and lower right of both images (marked). Hollow grains can be readily differentiated from capillary pores due to their angular, rectilinear shape, which is a pseudo-morph of the original anhydrous cement grain. Capillary pores are irregularly shaped (tortuous) and often appear to be connected, whereas hollow shells appear as isolated pores aiding in their identification.

3. Experimental: images and hollow grain features

One of the most important observations made thus far with the confocal technique is the existence of channels, which connect Hadley grains to areas of capillary pores located within

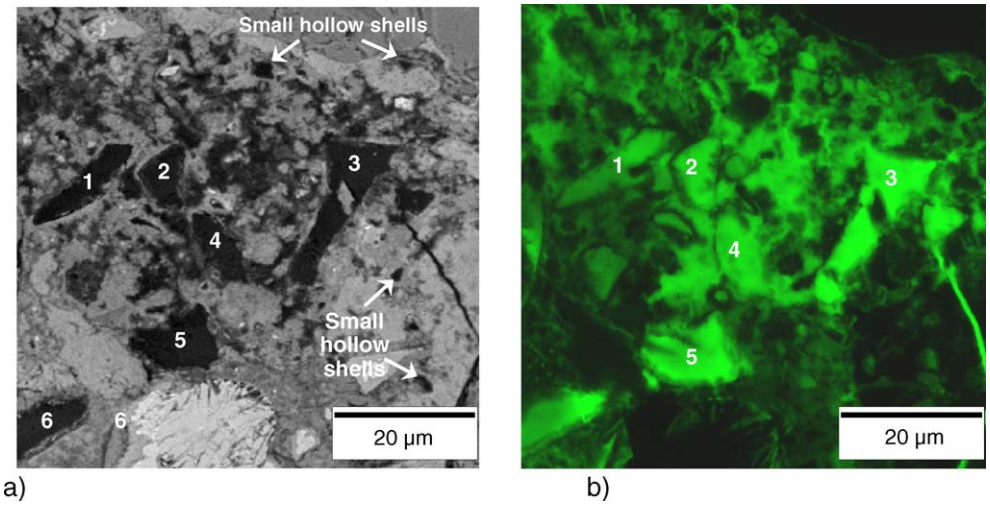

Fig. 1. Approximate area match between BEI and confocal images (specimen 0.6–28 d). Larger hollow shells marked 1–6. Note: Confocal image has been contrast enhanced to improve clarity for viewing. (a) BEI of specimen surface captured at ×1000 and cropped to area-match with confocal image set. Voids are black. (b) Top image in confocal *z*-stack image file. Note that voids in confocal images are areas of brightness.

HCP. These channels or connections were observed at depths below the specimen surface with no links to the surface, and did not therefore constitute specimen damage incurred during surface preparation. At some time during the specimen preparation process however, the impregnated features would have been connected to the surface via open pathways, i.e. by naturally occurring connected porous structures, or by damage (deep scratches, pull-outs, etc.) induced during specimen preparation. Resin would not have been able to reach these features if this were not the case. However any such surface structures were subsequently removed during later grinding/lapping and polishing procedures, leaving an underlying, undisturbed resin impregnated layer from which the images were obtained. The channels were observed to have varying morphology, with some appearing as large open, poorly defined features, and others appearing as very fine hair-like structures only extending for short distances away from reacted grains. Examples of both structure types are given in Figs. 2 and 3 below.

Fig. 2 comprises of a series of optical slices extracted from the confocal image stack. The images demonstrate how a large hollow shell exhibits complete rectilinear outer-shell morphology (dotted line in Fig. 2a, and marked by arrows in Fig. 2b–e) at a depth of approximately 0.88 μm below the top of the stack (approximate position of the specimen surface), with no breaks visible in the shell. At a depth of ~3.5 μm however, the hollow shell has grown in size and a large section of the outer shell has 'opened up' (circled in Fig. 2c–e) connecting the grain directly to surrounding capillary pores. Below this (at around 6 μm depth) the shell reappears and is evidently continuing at deeper levels, but the lower boundary of the grain is not seen. It was noticed that although large connecting channels were evident in both higher and lower w/c specimens, they mainly occurred in the higher (0.6) w/c specimen and at an early age; also these channels linked directly into large areas of capillary pores. In contrast, the image data from Fig. 3 illustrate pore channels of a very fine morphology which seem to occur at both ages.

Several connecting channels (labelled 'cc' in Fig. 3b and c) can be observed between different grains and capillary pores. The areas concerned are circled in Fig. 3a (top of image stack-specimen surface), where no sign of the deeper channels can be observed. In Fig. 3b (~3 μm below surface), a large capillary pore 'p' is located in the centre of the image, with small links 'cc' to two separate hollow shells 'h'. The form of this connecting structure is very similar in Fig. 3c, again forming links between hollow shells and capillary pores.

Both types of channel shown in Figs. 2 and 3 connect hollow Hadley grains with capillary pores, facilitating the transportation of fluids and ions, and it is noticeable that the connections are only seen to exist in areas adjacent to relatively large capillary pores as can be seen in Figs. 2 and 3. It is possible that these connections are actually an artefact of specimen

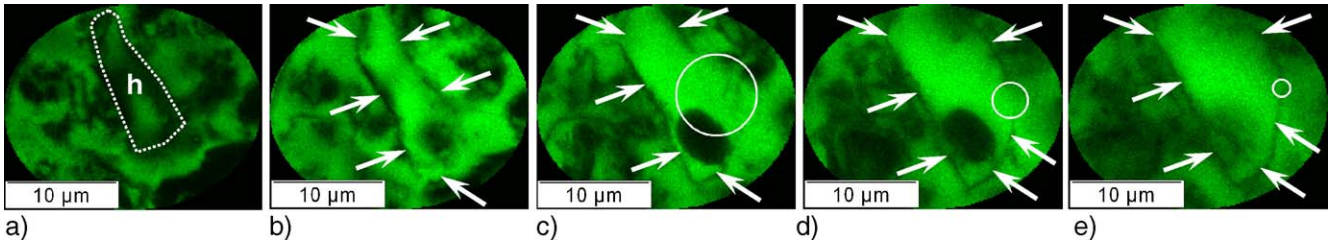

Fig. 2. 'Large' diffuse connection (marked in 'c–d') between hollow shell 'h' and capillary pores (0.6 w/c, 3 days). (a) slice 3/15 Depth=0.88 μm. (b) slice 6/15 Depth=2.19 μm. (c) slice 9/15 Depth=3.51 μm. (d) slice 12/15 Depth=4.82 μm. (e) slice 15/15 Depth=6.14 μm.

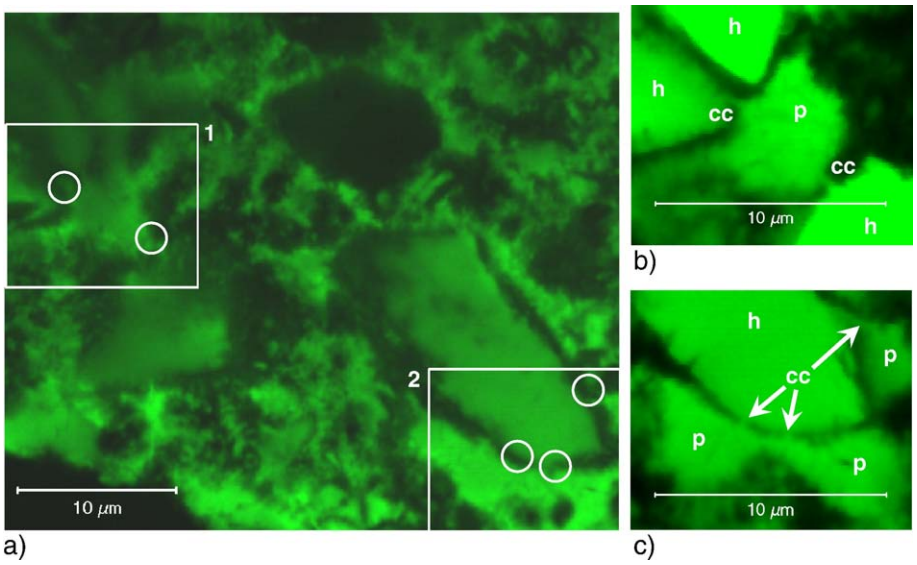

Fig. 3. Series of images showing very fine connecting channels (cc) between capillary pores 'p'and hollow shell cement grains 'h' below specimen surface (0.6 w/c, 28 days). (a) Top image in stack. Circles show where fine pore channels exist at lower depths. (b) Area 1 in (a) (3.08 μm below surface). (c) Area 2 in (a) (1.76 μm below surface).

preparation, i.e. micro-cracks that may have manifested themselves during the freeze-drying procedure prior to resin impregnation, as highlighted previously by Famy and co-workers [21–23]. It is also possible however that they are a 'natural' part of the microstructure, and further work is planned to investigate this point by comparing specimens at different ages that have been prepared with different drying and resin impregnation methods, and will be reported at a later date.

It was felt that further proof for the penetrability of hollow grains, independent of other structures such as micro-cracks, was necessary. Accordingly, further investigations of the image data were performed. It was soon realised that hollow shell cement grains, not visible on the surface, could be observed below specimen surfaces due to the semi-transparency of C–S–H and other reaction products. The laser probe has sufficient power to penetrate several micrometers of overlying material, and to excite fluorescent dye-filled voids lying below. Several grains were identified that were not observed to lie in the vicinity of micro-cracks and/or air voids.

Fig. 4 is an image gallery captured from specimen 0.4–28 d. The first image in the sequence is actually the third in the original sequence, which has been cropped laterally to give a 41×41 μm field of view, as well as being cropped horizontally by 0.88 μm from the original surface (upper two images removed). The gallery images are labelled sequentially and indicate actual depths below the specimen surface. The images show two different features of the porous microstructure. A large porous region has been circled in frame 1, which can be interpreted as a section through a hollow shell. In the following images this region is seen to increase in size, indicating that the hollow shell was sectioned through at a 'tip', as predicted in Section 1. This is a demonstration of the limitations imposed by 2D imaging (i.e. BEI) as was pointed out recently by Scrivener [24], where the true nature of 3D objects cannot be observed. The confocal technique however, is able to reveal the hollow shell in three dimensions, which is seen to possess internal anhydrous relics (observed in the second half of the data set). Other features (marked by arrows in Fig. 4) are small hollow shells that only appear well below the specimen surface, and are further evidence of connecting conduits between hollow shells and outer product C–S–H capillary porosity. The arrows mark the first instances on the z-axis where the hollow shells can be identified as autonomous objects, and where dark bands clearly delineate the hollow shell and its' morphology. Random pores do not have such a consistent morphology and are more tortuous in appearance as illustrated in Fig. 3b and c. From the relatively even distribution of arrows across the data set, it can be noted that the hollow shells are appearing regularly at nearly all levels throughout the imaging depth. However some of these may be the tips of larger hollow shells originally extending below the lower specimen surface, but lost when sectioning the specimen, i.e. an inverse situation to the region marked in Fig. 4 (frame 1). In total, eleven hollow shells have been marked in this way.

The images in Fig. 5 show evidence of a hollow grain, underlying a particle of uniform greyscale (marked by a white square). It was initially thought that this might be a hollow shell that had been sectioned through at a tip. However, further investigation revealed that the greyscale range for this particle was higher (greyscale ~160) than that measured for dense inner product C–S–H (greyscale ~150), but similar to the greyscale range of nearby calcium hydroxide (CH). X-ray microanalysis later confirmed that the calcium/silica ratio for this particle was in excess of the expected range for inner product C–S–H by a factor of about 5. It is likely therefore, that the particle is a sectioned area of CH formed within a void (although further quantitative data would be required to confirm this). Neither the BEI, nor the uppermost confocal image slice of this feature (Fig. 5a and b) reveal the presence of porosity within the feature, and cracks are not present. There is therefore no artificial or damage-formed conduit present, which would have

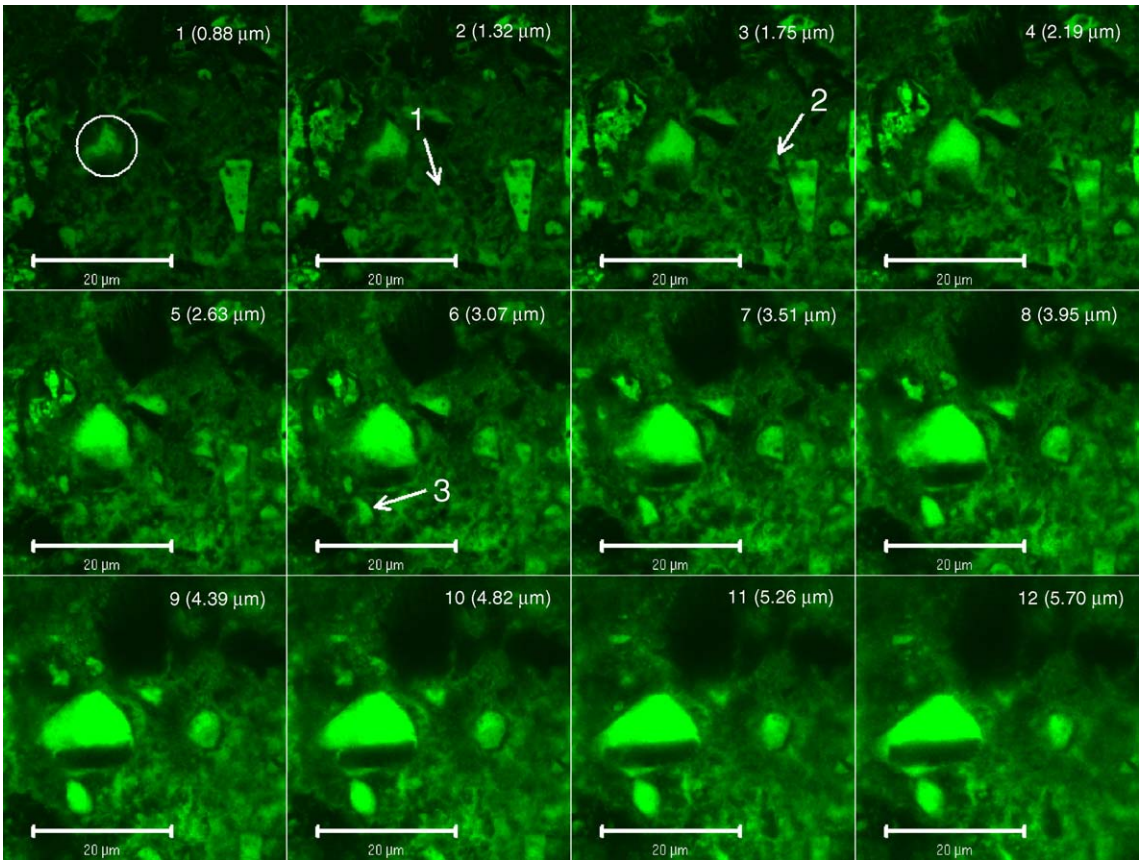

Fig. 4. Image gallery from confocal image stack, cropped to a selected region, showing the presence of hollow shells below a specimen surface. A larger shell has been sectioned through at a 'tip' (circled in frame 1), which increases in size as the focal plane of the microscope is moved deeper below the specimen surface. Three other hollow shells are marked in frames 2, 3 and 6, which are their first obvious appearance as hollow shells in the stack (specimen 0.4–28 d: Scale bars = 20 µm).

allowed resin to penetrate into the hollow shell grain, suggesting that resin was able to enter via naturally existing links with external capillary pores.

A partly reacted grain is also present in the centre of the backscattered image (indicated by arrow in Fig. 5a). Given the relatively uniform thickness of dense inner product C–S–H surrounding the partly reacted core, it is assumed that this grain has been sectioned in a place that passes through, or close to, a centre plane. The inner product C–S–H was measured to be approximately 3 µm thick using the centre of the total-grain region as the centre of gravity for measurement vectors (measurement lines radiating out from a central point here on a 2D plane). When the confocal image stack was subsequently measured through the *z*-axis, the difference in height from the top of the stack to the sub-surface hollow grain was also about 3 µm, suggesting a possibility that a shell had been sectioned in the vicinity of its uppermost surface.

Fig. 5b is a confocal image stack gallery, and shows the transition through CH that intersects the specimen surface (1st frame), to the appearance of the hollow shell cement grain at approximately 3 µm below the surface (8th frame). Fig. 5c reveals the hollow shell's sub-surface geometry by observing the 3D image stack in 'orthogonal' display mode, and shows the hollow shell to be rhombohedral in shape. The cross hairs in the centre of the shell indicate the position of the *x–z* and *y–z* planes. The smaller window to the top of the graphic represents an optical cross section of the *y–z* plane at this position, and the window to the right illustrates the same aspect for the *x–z* plane. The *x–y* image plane window in the centre of Fig. 5c shows the 11th frame in the stack (marked by the bold white frame border in Fig. 5b) located at a depth of ~4.4 µm, and its depth in the *y–z* and *x–z* windows is marked by dashed lines as the '*Z* position'. The *z*-position of the *x–y* plane at this depth can be observed to lie below the overlying CH, which has been marked. Points ABCD indicate the corners of the hollow shell. Line 1 represents a vertical plane linking points B and C, and line 2 indicates a parallel plane between points A and D. Lines 3 and 4 represent planes AB and CD, respectively. Planes AB, AD, and BC can be observed by thin dark lines that delineate the hollow shell. Plane CD however is more diffuse at its intersection with the *x–y* image plane, and appears less well defined (all planes are marked and labelled accordingly).

Interestingly, the CH region seems to be more laterally extensive in the *y–z* plane where the hollow shell surfaces planes 1 and 2 are almost normal to the specimen surface, compared to the *x–z* plane where the hollow shell surfaces planes 3 and 4 are oriented at approximately 45° to the specimen surface. Indeed, plane 3 does not extend to the CH region at this point along the *x* axis, which could provide an explanation for the access of resin

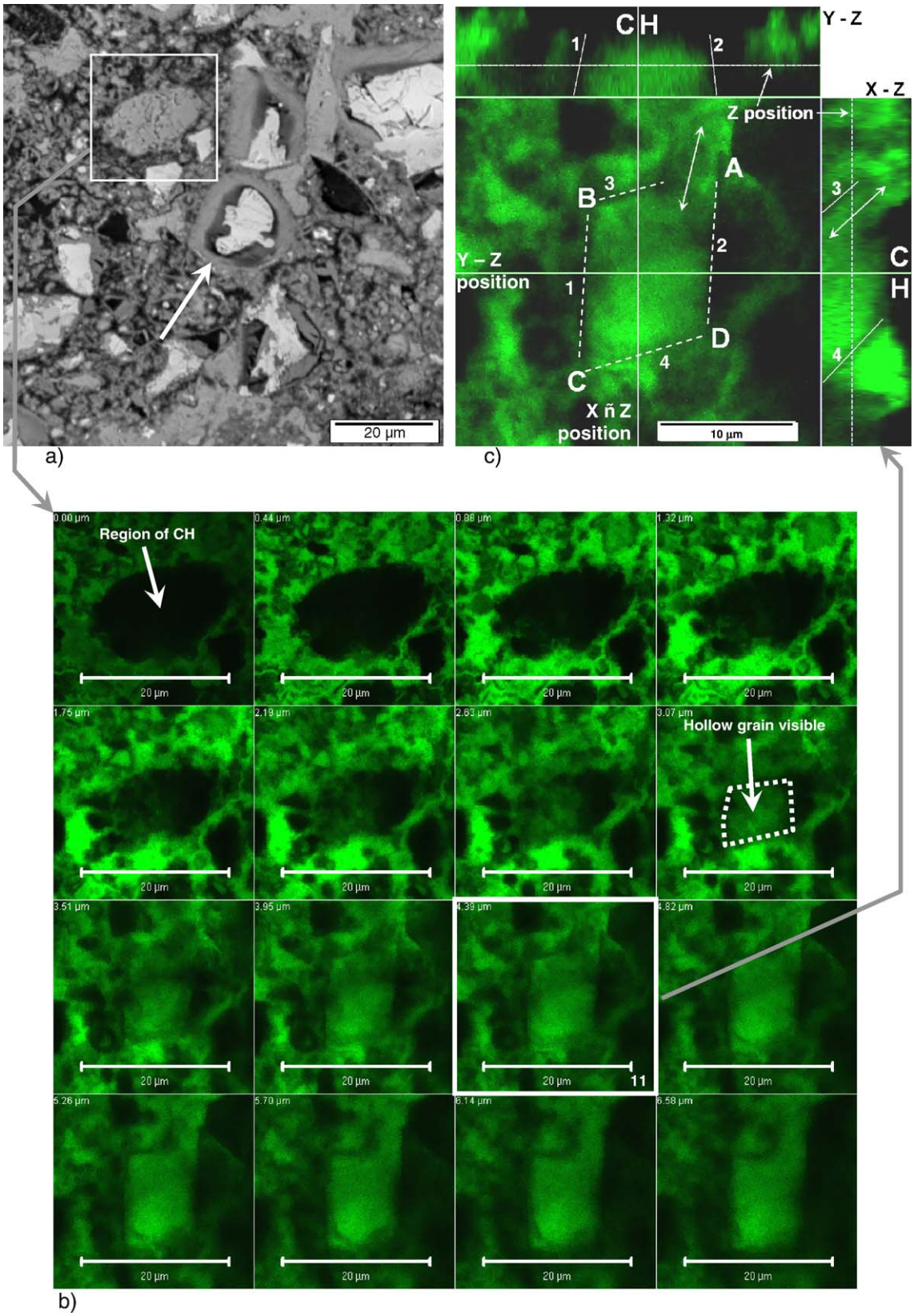

Fig. 5. Image set showing CH overlying hollow shell cement grain (specimen 0.4–3 d). (a) BEI of specimen surface with hollow shell grains (arrow) and CH (box) formed in voids. (b) Cropped confocal data set of region marked on (a), showing sub-surface imaging through CH to hollow shell grain. Total imaging depth = 6.58 µm. (c) Orthogonal sectioning of image stack from frame 11, (highlighted in (b)). Contrast enhanced to help view outline of hollow shell grain below CH (see text for annotations).

into and out of the hollow shell, as indicated by the double headed arrows in both the *x–z* and *x–y* (main) windows.

4. Conclusions

1. Three-dimensional imaging of hollow shell cement grains is possible by LSCM however more development work is required to improve image resolution, penetration depth, and data interpretation. The work presented here has concentrated on interpretation of hollows shell cement grains and the existence of possible links between them and capillary pores, which adds to the features identified reported in our initial study (natural aggregate interfaces, capillary pores, partly reacted cement grains and micro-cracks).
2. Resin impregnation and imaging of hollow shell cement grains well (~6 μm) below the specimen surface, shows that hollow shells are connected to HCP capillary pores by channels, supporting molecular transport. The formation of these channels is not understood and they could be either naturally occurring or damage induced.
3. 3D confocal imaging has confirmed sectioning of grain tips during specimen surface preparation. These 'tips' would normally be categorised as smaller hollow shell grains if only 2D surface imaging was performed.

This work is part of an exploratory study using fluorescent laser scanning confocal microscopy. Future work will aim to improve image clarity at capture and by processing with image filters, develop methods for thresholding 3D structures, investigate the 3D geometry and connectivity of capillary pores, attain a better understanding of image features and their occurrences, and develop models for quantification of 3D pore connectivity.

Acknowledgements

We would like to acknowledge the support provided under EPSRC grant M97206, and to the Department of Biochemistry at Imperial College London for access to their confocal microscope.

References

[1] D. Hadley, The nature of the paste–aggregate interface, Ph.D. Thesis, Purdue University, (1972) 173 pp.
[2] T.C. Powers, PCA research and development laboratories, Portland Cement Association 3 (1) (1961) 47–55.
[3] K.L. Scrivener, The use of backscattered electron microscopy and image analysis to study the porosity of cement paste, in: L.R. Roberts, J.P. Skalny (Eds.), Pore Structure and Permeability of Cementitious Materials, Materials Research Society, vol. 137, 1989, pp. 129–140.
[4] K.O. Kjellsen, H.M. Jennings, B. Lagerblad, Evidence of hollow shells in the microstructure of cement paste, Cement and Concrete Research 26 (4) (1996) 593–599.
[5] K.O. Kjellsen, B. Lagerblad, H.M. Jennings, Hollow shell formation—an important mode in the hydration of Portland cement, Journal of Materials Science 32 (1997) 2921–2927.
[6] K.O. Kjellsen, E.H. Altlassi, Pore structure of cement silica fume systems: presence of hollow-shell pores, Cement and Concrete Research 29 (1999) 133–142.
[7] S. Diamond, Aspects of concrete porosity revisited, Cement and Concrete Research 29 (1999) 1181–1188.
[8] S. Diamond, Cement paste microstructure in concrete, in: L.J. Struble, P.W. Brown (Eds.), Microstructural Development During Hydration of Cement, Boston, Massachusetts, 1986, Mat. Res. Soc. Symp. Proc., vol. 85, 1987, pp. 21–31.
[9] R.B. Williamson, Solidification of Portland Cement, Report No. UC-SESM 70-23, University of California, Berkeley, 1970, 109 pp.
[10] K.L. Scrivener, E.M. Gartner, Microstructural gradients in cement paste around aggregate particles, in: S. Mindess, S.P. Shah (Eds.), Bonding in Cementitious Composites, Materials Research Society, vol. 114, 1988, pp. 77–86.
[11] K.L. Scrivener, A.K. Crumbie, P.L. Pratt, A study of the interfacial region between cement paste and aggregate in concrete, in: S. Mindess, S.P. Shah (Eds.), Bonding in Cementitious Composites, Materials Research Society, vol. 114, 1988, pp. 87–88.
[12] M.K. Head, N.R. Buenfeld, Confocal imaging of porosity in hardened concrete, Cement and Concrete Research 36 (5) (2006) 896–911.
[13] D.A. Lange, H.M. Jennings, S.P. Shah, Analysis of surface roughness using confocal microscopy, Journal of Materials Science 28 (14) (1993) 3879–3884 (Chapman and Hall).
[14] B. Walk-Lauffer, R. Bornemann, D. Knöfel, E. Thiel, In situ observation of hydrating cement-clinker phases by means of confocal scanning microscopy—first results, 24th International Congress on Cement Microscopy, 2002, pp. 95–106.
[15] K.E. Kurtis, N.B. El-Askar, C.L. Collins, N.N. Naik, Examining cement-based material by laser scanning confocal microscopy, Cement and Concrete Composites 25 (7) (2003) 695–701 (Elsevier Science Ltd).
[16] C.L. Collins, J.H. Ideker, K.E. Kurtis, Laser scanning confocal microscopy for in situ monitoring of alkali–silica reaction, Journal of Microscopy 213 (2) (2004) 149–157 (The Royal Microscopical Society).
[17] N. Petford, G. Davidson, J.A. Miller, Pore structure determination using confocal scanning laser microscopy, Physics and Chemistry of the Earth (A) 24 (7) (1999) 563–567 (Elsevier Science Ltd).
[18] B. Menendez, C. David, A.M. Nistal, Confocal scanning laser microscopy applied to the study of pore and crack networks in rocks, Computers and Geosciences 27 (2001) 1101–1109 (Elsevier Science Ltd).
[19] J.T. Fredrich, 3D imaging of porous media using laser scanning confocal microscopy with applications to microscale transport processes, Physics and Chemistry of the Earth (A) 24 (7) (1999) 551–561 (Elsevier Science Ltd).
[20] B. Menendez, C. David, M. Darot, A study of the crack network in thermally and mechanically cracked granite samples using confocal scanning laser microscopy, Physics and Chemistry of the Earth (A) 27 (7) (1999) 627–632 (Elsevier Science Ltd).
[21] C. Famy, K.L. Scrivener, A.K. Crumbie, What causes differences of C–S–H gel grey levels in backscattered electron images? Cement and Concrete Research 32 (9) (2002) 1465–1471 (Elsevier Science Ltd).
[22] C. Famy, K.L. Scrivener, A. Atkinson, A.R. Brough, Effects of an early or a late heat treatment on the microstructure and composition of inner C–S–H products of Portland cement mortars, Cement and Concrete Research 32 (2) (2002) 269–278 (Elsevier Science Ltd).
[23] C. Famy, K.L. Scrivener, A. Atkinson, A.R. Brough, Influence of the storage conditions on the dimensional changes of heat-cured mortars, Cement and Concrete Research 31 (5) (2001) 795–803 (Elsevier Science Ltd).
[24] K.L. Scrivener, Backscattered electron imaging of cementitious micro-structures: understanding and quantification, Cement and Concrete Composites 26 (2004) 935–945 (Elsevier Science Ltd).